# Assessment of Singularities in the EEG During A-Phases of Sleep Based on Wavelet Decomposition

D. I. Medina-Ibarra, I. Chouvarda, *Senior Member, IEEE*, J. S. Murguía, Alfonso Alba, Edgar R. Arce-Santana, Anna M. Bianchi, *Senior Member, IEEE*, and Martin O. Mendez

***Abstract*— Electroencephalography (EEG) signals convey information related to different processes that take place in the brain. From the EEG fluctuations during sleep, it is possible to establish the sleep stages and identify short events, commonly related to a specific physiological process or pathology. Some of these short events (called A-phases) present an organization and build up the concept of the Cyclic Alternating Pattern (CAP) phenomenon. In general, the A-phases abruptly modify the EEG fluctuations, and a singular behavior could occur. With the aim to quantify the abrupt changes during A-phases, in this work the wavelet analysis is considered to compute Hölder exponents, which measure the singularity strength. We considered time windows of 2s outside and 5s inside A-phases onset (or offset). A total number of 5121 A-phases from 9 healthy participants and 10 patients with periodic leg movements were analyzed. Within an A-phase the Hölder numerical value tends to be 0.6, which implies a less abrupt singularity. Whereas outside of A-phases, it is observed that the Hölder value is approximately equal to 0.3, which implies stronger singularities, i.e., a more evident discontinuity in the signal behavior. In addition, it seems that the number of singularities increases inside of A-phases. The numerical results suggest that the EEG naturally conveys singularities modified by the A-phase occurrence, and this information could help to conceptualize the CAP phenomenon from a new perspective based on the sharpness of the EEG instead of the oscillatory way.**

***Index Terms*— Cyclic alternating pattern, EEG, scaling exponent, singular behavior, sleep, wavelet transform.**

Manuscript received 26 February 2022; revised 26 July 2022; accepted 5 September 2022. Date of publication 13 September 2022; date of current version 29 September 2022. This work was supported in part by the Scholarship Granted by the Consejo Nacional de Ciencia y Tecnología (CONACYT) under Grant 2019-000037-02NACF and Grant CB 2017-2018 A1-S-45697. *(Corresponding author: J. S. Murguía.)*

D. I. Medina-Ibarra is with the Universidad Autónoma de San Luis Potosí, San Luis Potosí 78000, Mexico (e-mail: davidmedinai@hotmail.com).

I. Chouvarda is with the Laboratory of Computing, Medical Informatics and Biomedical Imaging Technologies, School of Medicine, Aristotle University of Thessaloniki, 541 24 Thessaloniki, Greece (e-mail: ioanna@med.auth.gr).

J. S. Murguía, Alfonso Alba, and Edgar R. Arce-Santana are with the Laboratorio Nacional-Centro de Investigación, Instrumentación e Imagenología Médica, Facultad de Ciencias, Universidad Autónoma de San Luis Potosí, San Luis Potosí 78000, México (e-mail: ondeleto@uaslp.mx; alfonso.alba@uaslp.mx; arce@fciencias.uaslp.mx).

Anna M. Bianchi is with the Dipartimento di Elettronica, Informazione e Bioingegneria, Politecnico di Milano, 20133 Milan, Italy (e-mail: annamaria.bianchi@polimi.it).

Martin O. Mendez is with the Laboratorio Nacional-Centro de Investigación, Instrumentación e Imagenología Médica, Facultad de Ciencias, Universidad Autónoma de San Luis Potosí, San Luis Potosí 78000, México, and also with the Dipartimento di Elettronica, Informazione e Bioingegneria, Politecnico di Milano, 20133 Milan, Italy (e-mail: mmendez@fc.uaslp.mx).

Digital Object Identifier 10.1109/TNSRE.2022.3205267

## I. Introduction

SLEEP is a fundamental process for any human being. During sleep, different activities such as memorization, resting, and growing, generally occur. However, sleep could be interrupted by different sources, both internal or external to the body. For instance, the internal sources could be derived from apnea episodes or mental stress, while the external ones are related to lights, environmental noise, or other disturbances. Sleep interruptions caused by these sources may result in fragmented sleep, which is reflected as social and physiological problems. Among the most representative problems, we can find metabolic syndrome [1], irritability, lack of concentration and traffic accidents [2], [3]. The main clinical tool for sleep evaluation is polysomnography (PSG), which is based on the recording of bio-electrical signals, including electroencephalogram (EEG), electrooculogram (EOG) and electromyogram (EMG). These biosignals are used to identify the sleep stages: rapid eye movement (REM) and non-rapid eye movement (NREM). These stages alternate across the sleep time producing cycles that have a duration between 90-120 minutes. Also, the NREM stage is subdivided into four stages denoted as S1, S2, S3 and S4. Although the PSG test uses several signals to assess sleep quality, the EEG signal is often the main reference because it contains five main rhythms (Delta, Theta, Alpha, Beta, and Gamma) which are useful in determining the sleep stages [4]. Nevertheless, in recent years some experts have observed that there are short and recurrent events in the EEG that interrupt its basal rhythms. These events, called A-phases, present rapid EEG changes in frequency and amplitude. A-phases present duration between 2-60 seconds; and there is evidence of a significant correlation with the sleep stage transitions [3]. It seems that A-phases participate in the sleep stage continuity. The A-phases are grouped into three types based on their spectral characteristics and duration, as described below:

- A1-phase: Characterized by bursts and K-complexes of Delta waves (0.5 Hz - 4 Hz).
- A2-phase: Presents rapid EEG waves (Alpha (8 Hz - 12 Hz) and Beta (12 Hz - 30 Hz)) that

cover between 20% and 50% of the A-phase duration and the Delta waves in the rest of the event duration.
- A3-phase. Characterized by Alpha and Beta waves, which occupy more than 50% of the A-phase duration.

Also, from the A-phase occurrence, we can visualize an oscillatory pattern, called Cyclic Alternating Pattern (CAP) from sleep [5], that helps to measure the sleep quality employing the ratio between the CAP time and total sleep time, named CAP rate index [6]. Regardless of the importance of the CAP rate for sleep evaluation, the A-phase scoring is visually performed by a clinical expert. CAP evaluation requires the annotation of approximately 300 A-phases, and as a consequence, this procedure is tedious, with large subjectivity and high inter-scorer variability [7].

Many works have been published with the goal of quantifying the A-phases characteristics, which may allow implementing computational methods for clinical support during the annotation process [8]. However, until the present time, the automatic annotation remains an open topic. In order to improve this process, the research of quantitative measures of the EEG, capable of distinguishing the A-phases from the background, is desirable.

Navona *et al.* developed an automatic method for A-phases detection based on the extraction of different descriptors by using a bank of band-pass filter, where each descriptor corresponds to a different EEG frequency band. The computation of these descriptors, followed by the superimposition of two thresholds and the application of logical criteria, provided a good performance [9]. A similar methodology to recognize A-phases from the background was used by Barcaro *et al.* and they reported a good accuracy for the A-phase detection [10]. With similar features, Mariani *et al.* trained different types of classifiers, such as linear and quadratic discriminant, boosting neural networks, support vector machines, and adaptive boosting [8], [11].

In addition, a group of statistics (standard deviation, mode, kurtosis, and skewness), frequency (power in the characteristic EEG frequency bands) and complexity (LZC, FD, sample entropy, and Tsallis entropy) features were evaluated by Mendez *et al.*, which were used as input in the k-nearest neighbors classifier to show the ability to discriminate an EEG segment between the onset of A-phase and the background with a good accuracy [12]. Some authors applied time-frequency methods for feature extraction, for instance, Dhok *et al.* used Wigner-Ville Distribution and Rényi entropy in consecutive 2-s segments and to fed with these parameters a support vector machine to determine if each segment corresponds to an A-phase or background [13]. Recently, Fantozzi *et al.* introduced an alternative approach that consists of generating features from EEG based on a bank of band-pass filters over segments of 90s and divided into epochs of 30s. For each frequency band and for each such epoch, the root mean square of the signal was computed and a threshold was used as 1.5 RMS. Each epoch was identified and marked when the variability measure 1.6 times higher than the variability of the segment. This process was applied in each derivation of EEG ( F2-F4/Fp2-F4, F4-C4, C4-P4, P4-O2, C4-A1, and F4-A1) with interesting results using the F4-C4 derivation [14].

In recent years, some studies have used techniques based on deep learning to detect and characterize A-phases. Arce-Santana *et al.* and Murarka *et al.* used frequency and temporal features, respectively, from the EEG signal across consecutive segments to train a convolutional neural network to determine whether the segment belongs to an A-phase [15], [16]. Finally, Hartmann *et al.* and Mendonça *et al.* have used a long short-time memory neural network to include temporal relation across EEG signal. They obtained features similar to previous works and used them to feed the classifier [17], [18]. In general, all these studies have reported interesting results, however, there is a lack in the correct detection in the onset/offset and alternative techniques that provide a complementary characterization of the transitions between the A-phases and the background activity are needed.

In fact, singularities or irregular structures can convey essential information [19]. Within clinical applications, many biological signals present irregular patterns or behaviors that may be related to a condition of interest; therefore, it may be useful to study this kind of structures as part of a health diagnosis. For instance, A-phases produce a short and fast change in the EEG amplitude [12], whose magnitude was defined by Terzano *et al.* [5] as one-third of the basal amplitude. In fact, the amplitude change is commonly used as an important feature in algorithms to automatically detect the A-phases [8]. Since the abrupt transition occurs in small time intervals or at specific points, a local analysis of this change is required. Moreover, it is often unclear whether this fast change is related to a singularity, and numerical quantification of this change could unveil previously unobservable characteristics. Thus, it could be interesting to understand whether the appearance of singularities in the EEG is related to the occurrence of A-phases. In general, it is known that the EEG signals present fast amplitude and frequency changes which can be related to singularities [20], but they have not been associated to specific events.

In the biomedical field, singularities may reveal relevant information about the physiological systems, e.g. the respiratory system [21], [22], cardiac function [23], [24] and muscular activity [25], [26]. Some methods based on time and frequency domains have been developed and used for singularity detection. One of the common tools to analyze singularities or irregular structures is the Fourier Transform [27]. However, this transform yields a global characterization of the regularity of a mono-component signal. In multi-component signals (where frequency changes occur at a certain time) the Fourier Transform may be used to determine the frequency components but the time localization of the frequency change (i.e., the singularity) is lost.

The singularity temporal localization problem can be circumvented by Wavelet decomposition throughout the asymptotic decay at the different scales. This decomposition allows one to evaluate the local regularity or smoothness of a signal through a real number called the Hölder exponent [27], [28], [29], which can be computed in the time-scale plane by using the Wavelet Transform Modulus Maxima (WTMM).

In this paper, we present a systematic method to evaluate the local singularities in the EEG signal during the A-phase occurrences. The proposed method is based on the wavelet

analysis to estimate the Hölder exponents, from which two quantitative indices are derived, and the method is robust to the Gaussian noise, which commonly affects biomedical signals. Another contribution is to show that these indices are modulated by the presence of an A-phase in a way that is statistically significant.

## II. Methods

### A. Data Description

This study was carried out on two groups, the healthy group (HLT) that consists of 9 recordings (three males and six females) without sleep complaints, and the pathologic sleep group that includes 10 pathological subjects (seven males and three females) with Periodic Leg Movements (PLM). The subjects ages range between 23 and 37 years for the HLT group, and between 40 and 62 years, for the PLM group. The PLM pathology was chosen for this study because the database has a sufficient number of subjects and the necessary conditions (sampling frequency, duration of the recording and number of A-phases).

HLT and PLM recordings belong to the open Physionet CAP Sleep Database (https://physionet.org/content/capslpdb/1.0.0/). CAP Sleep Database is a collection of 108 polysomnographic recordings acquired at the Sleep Disorder Center of the Ospedale Maggiore of Parma, Italy. EEG was recorded from a C3/A2 or a C4/A1 derivation integrated by bipolar montages (Fp1-F3, F3-C3, C3-P3, P3- O1, Fp2-F4, F4-C4, C4-P4, P4-O2) used to score CAP phenomenon. Each recording is composed of at least three EEG channels, electromyography, electrooculographic channels, respiratory signal and, electrocardiogram. The recordings were recorded with a sampling rate of 100, 128, 200, 256, or 512 Hz.

Embla REMlogic software was used to score and visualize all polysomnographic recordings, where the scores for each recording were saved as text files. Score files have the following fields: Sleep stage (W=wake, S1-S4=sleep stages, R=REM, MT=body movements), Body position (Left, Right, Prone, or Supine; not recorded in some subjects), Time of the day [hh:mm:ss], Event (either sleep stage (SLEEP S0-S4, REM, MT), A-phase, Duration (in seconds) and Location (the signals in which the event can be observed). All the annotations were revised by an expert physician in the area based on the gold standard rules [4], [5].

In this study, we are interested in evaluating the singularities around the onset and offset of A-phases in subjects that present a normal and pathological sleep macro-structure, focusing on a single pathology PLM. The Table I shows the general information such as age, sleep stages, number and duration of A-phases from all recordings used in this study. Also, information about the number of A-phases, sleep time spent in A-phases, and duration for each A-phase type is found.

### B. Data Encoding

The sampling frequency of most of the signals used to carry out this study is 512 Hz; however, some signals had sampling frequencies below 512 Hz. Signals with a sampling frequency equal or higher than 200 Hz were upsampled to 512 Hz using cubic spline interpolation, since we are looking for abrupt transitions that can only be represented by a higher sampling rate. Subsequently, we perform the extraction of EEG segments for each type of A-phase per recording. We focused on the onset and offset instants of the A-phase occurrence. Thus, each segment consists of two seconds before the A-phase onset and five seconds of the A-phase onset (seven seconds in total). A similar process is performed for the A-phase offset. We extract segments of five seconds of the A-phase offset and two seconds after the A-phase offset. The rationale behind the decision for the specific segment size is to study the singularities of the EEG signals around the A-phase and not only to evaluate the specific time instant of the onset and offset. As a consequence, A-phases with a duration of less than five seconds were not considered. Please note that a large quantity of the A-phases presents a duration greater than 5 seconds, see Table I.

Fig. 1 shows an example of the EEG signal during one A-phase. The box function (orange line) is the clinical annotation and represents the length of an A-phase. The arrow in the upper part of the figure shows the seconds related to the background activity ($S_{n-1}, S_{n-2}, S_{m+1}, S_{m+2}$) and the ones belonging to the A-phase ($S_n$ for onset and $S_m$ for offset). Note that these segments are used in the analysis.

Also, to verify if the sleep stage activity modifies the behavior of singularities produced by the A-phases, the A-phases were analyzed separately in two groups: light sleep (stages S1 and S2) and deep sleep (stages S3 and S4).

### C. Wavelet Singularity Analysis

In many situations, signals contain valuable information in their transient characteristics and singular structures. To quantify the singularities in a signal is necessary to consider the local regularity of such a signal, which can be measured by the Hölder exponent $\alpha$. The wavelet transform (WT) has been demonstrated to be a successful and suitable tool to estimate the Hölder exponents, because the multiscale decompositions implied by the WT are well adapted to evaluate scaling properties, and numerically is more stable than other methods [19].

In the following we shortly describe the relationship between the WT and Hölder exponents. Let $n$ be a positive integer and $\alpha$ be in the interval $n \leq \alpha < n+1$. A function $f(t)$ is said to be Hölder $\alpha$ at $t_0$ if and only if there exist a constant $A > 0$ and a polynomial $P_n(t)$ of order $n$, such that

$$|f(t) - P_n(t - t_0)| \leq A\,|t - t_0|^{\alpha}\,. \tag{1}$$

Consequently, a function $f(t)$ is uniformly Hölder, over the interval $[a, b]$, if there exist a constant $A > 0$ and a polynomial $P_n(t)$ of order $n$, for which the previous equation holds for all $t, t_0 \in [a, b]$.

In order to detect and measure the singularities of a signal, Mallat and Hwang [19] considered a method, which is in terms of the decay/growth rate the wavelet coefficients. The reader is referred to Appendix of this paper for a short introduction of continuous wavelet transform. However, the decay rate can be measured from the set of points where the wavelet modulus reaches the local maxima values. In other words, the singularities of a signal can be detected by finding the

TABLE I

MEAN AND STANDARD DEVIATION OF GENERAL SLEEP INDEXES (MACRO- AND MICRO-STRUCTURES) FOR DATABASE UTILIZED IN THIS STUDY

| | | | A-Phase | | | Macrostructure | | | |
|---|---|---|---|---|---|---|---|---|---|
| | Subjects | Age | No | Time (s) | Duration (s) | NREM (h) | REM (h) | WAKE (h) | RECORDING (h) |
| HLT | 9 | 31.6±5.2 | 419±96.8 | 3366.3±588 | 8.03±5.5 | 5.7±0.8 | 1.8±0.6 | 0.8±0.5 | 8.3±0.6 |
| PLM | 10 | 55.1±6.7 | 455±114 | 4078±805.7 | 8.9±6.5 | 4.7±0.75 | 1.2±0.6 | 1.6±1.3 | 7.6±1.5 |
| | No. A-phases | | | Total Time in A-Phase of A-phases (s) | | | Time of A-Phase(s) | | |
| | A1 | A2 | A3 | A1 | A2 | A3 | A1 | A2 | A3 |
| A-phases (HLT) | 254±104 | 87±38.4 | 77.5±19 | 1583±652 | 737±316.2 | 1046±179 | 6.2±3.0 | 8.5±4.65 | 13.5±8.6 |
| A-phases (HLT) $> 5s$ | 120±51 | 61±33 | 68±15 | 1030±495 | 630±313 | 1005±184 | 8.6±2.8 | 10.3±4.5 | 14.8±8.3 |
| A-phases (PLM) | 204±77.3 | 98±36 | 152±47.9 | 1149±517 | 820±278 | 2109±600 | 5.6±2.75 | 8.3±4.2 | 13.8±8.1 |
| A-phases (PLM) $> 5s$ | 78±45.5 | 71±23 | 140±41.9 | 648±390 | 700.8±235 | 2053±591 | 8.3±2.7 | 9.9±4 | 14.7±8 |

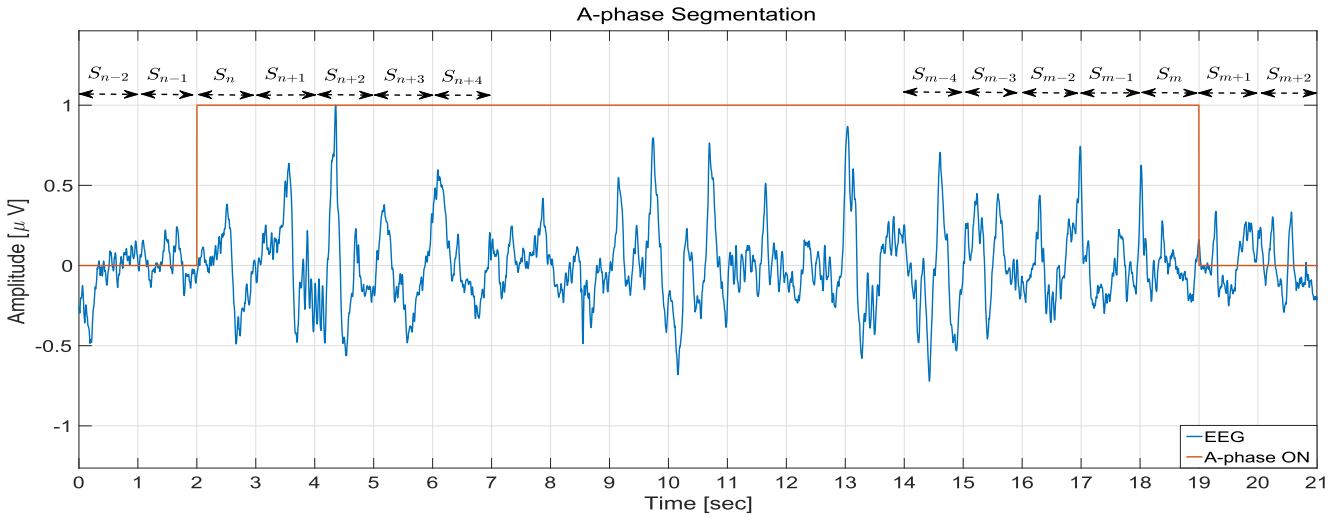


Fig. 1. Example of a segment of the EEG signal during the occurrence of an A-phase. The orange line defines the clinical annotation.

abscissa where the wavelet modulus maxima converge at fine scales. Any connected curve in the scale - time plane $(s, t)$ along which all points are modulus maxima is called a maxima line [27]. The previous method is called the wavelet transform modulus maxima (WTMM), and the regularity of a signal can be determined by the decay of the maxima line generated by the evolution of the WTMM at a given time point. The measure of this decay is the Hölder exponent of the signal at a specific point. Therefore, by examining the exponent in time, singularities can be localized.

It is worth to say that a signal without oscillations in a neighborhood of the singularity means that it has an isolated singularity. To quantify such a singularity, let $f(t)$ be a signal whose wavelet transform is well defined over $(a, b)$ and let $t_0 \in (a, b)$. Suppose there exists a scale $s_0 > 0$, and a constant $C$, such that for $t \in (a, b)$ and $s < s_0$, all the modulus maxima of $W_f(s, t)$ belong to a cone of influence given by $|t - t_0| \leq Cs$ (see the Appendix for the definition of the cone of influence). Then the function $f(t)$ has a Hölder exponent, $\alpha \in (n, n + 1)$ at $t_0$, if and only if there exists a constant $A > 0$ such that at each modulus maxima $(s, t)$ in the cone of influence $|t - t_0| \leq Cs$ one has

$$\left|W_f(s,t)\right| \leq As^{\alpha+\frac{1}{2}}, s \to 0, \tag{2}$$

which is equivalent to

$$\log_2 \left|W_f(s,t)\right| \leq \log_2 A + \left(\alpha + \frac{1}{2}\right) \log_2 s. \tag{3}$$

The Hölder exponent $\alpha$ is numerically computed from (3) with a linear regression of $\log_2 \left|W_f(s,t)\right|$ as a function $\log_2 s$. The analyzing wavelet functions which are most used for this kind of analysis are the successive derivatives of the Gaussian function $\psi^{(n)}(t) = \frac{d^n}{dt^n}(exp(-t^2/2))$, $n \in Z^+$, because they are well localized both in space and frequency, and they have the same number of vanishing moments as the order of derivative, a crucial property to detect singularities.

### D. Simulations for the Effect of Noise

Biomedical signals present a certain level of high-frequency noise which is added during the acquisition process. The nature of the noise is related to different factors such as electromagnetic interference, amplification, and digitalization [17]. This high-frequency noise can produce singularities in the signal and, as a consequence, the results of the singularity analysis could be corrupted or degraded. One way to mitigate the problem is to filter the signal; however, the filtering process smooths the signal and the singularities of interest may disappear. With the aim to analyze the effect of the high-frequency noise in the computation of singularities, we added Gaussian noise to two simple signals with known singularity.

The first signal is the step function $u(t)$, which is defined as:

$$u(t) = \begin{cases} 0, & t < 0 \\ 1, & t \geq 0 \end{cases} \tag{4}$$

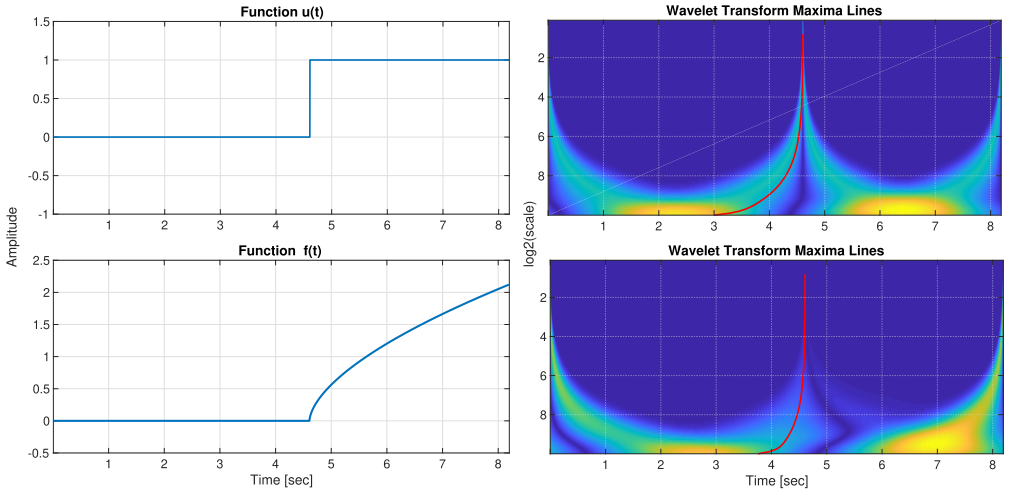


Fig. 2. Left column illustrates the synthetic signals and the right column shows the respective wavelet transform. The red lines correspond to the Maxima Modules that defines Hölder exponent $\alpha$.

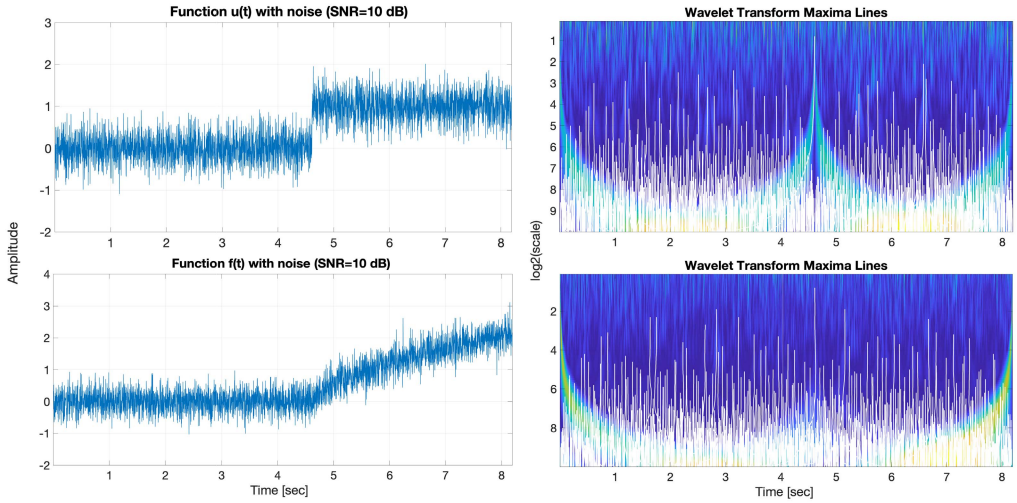


Fig. 3. Left column illustrates the synthetic signals contaminated with Gaussian noise and the right column shows the respective Wavelet Transform Modules Maxima. Note that the high levels of noise produce many spurious singularities, which can be confounded with the true singularity.

It is clear that $u(t)$ is singular and not differentiable at $t = 0$. The second signal under study is defined as:

$$f(t) = \begin{cases} 0, & t < 0 \\ t^{0.6}, & t \geq 0 \end{cases} \tag{5}$$

For this signal, the value of the derivative is indeterminate at $t = 0$. The signals were generated with a sampling rate of $f_s = 512$ Hz with $-4 < t < 4$. Fig. 2 shows the signals and their WTMM based on the second derivative of the Gaussian mother wavelet. The red line defines the Maxima Modules that are used to compute the Hölder exponent. Note the red line moves from the large to small scales as $t$ approaches to the singularity.

Subsequently, Gaussian noise was added with a signal-to-noise ratio (SNR) in the interval [10 dB, 50 dB] in steps of 5 dB. Once the noise was added to the signals, we computed the Hölder exponent through the WTMM. The procedure was performed 100 times (using different noise realizations) for each SNR level. Fig. 3 shows the noise effect, where a large number of spurious singularities can be observed; however, the singularity of interest remains in the expected location and it can be distinguished from spurious singularities produced by noise.

The mean of Hölder exponent $\alpha$, and its concentration (in windows, with one-second resolution), were computed for each realization of noise. The results of all the realizations were averaged. This procedure was applied to each noise level. (The definitions of the mean of Hölder exponent and its concentration are described in EEG singularity analysis section).

### *E. Statistical Analysis*

The $\alpha$ behavior was analyzed inside and outside the A-phases, with one second resolution. For the onset case, the first two seconds have the singularities of the basal oscillations corresponding to the current sleep stage while the following five seconds belong to the A-phase. In the offset case, the first five seconds are inside the A-phase and the last two seconds belong to the basal stage. A comparison of the mean $\alpha$ value among windows was carried out. This comparison was made for each A-phase sub-type (A1-, A2-, and A3-phase) in the onset and offset cases. The wilcoxon signed-rank test was used for the comparison. A $p$-value of 5 % was used to define

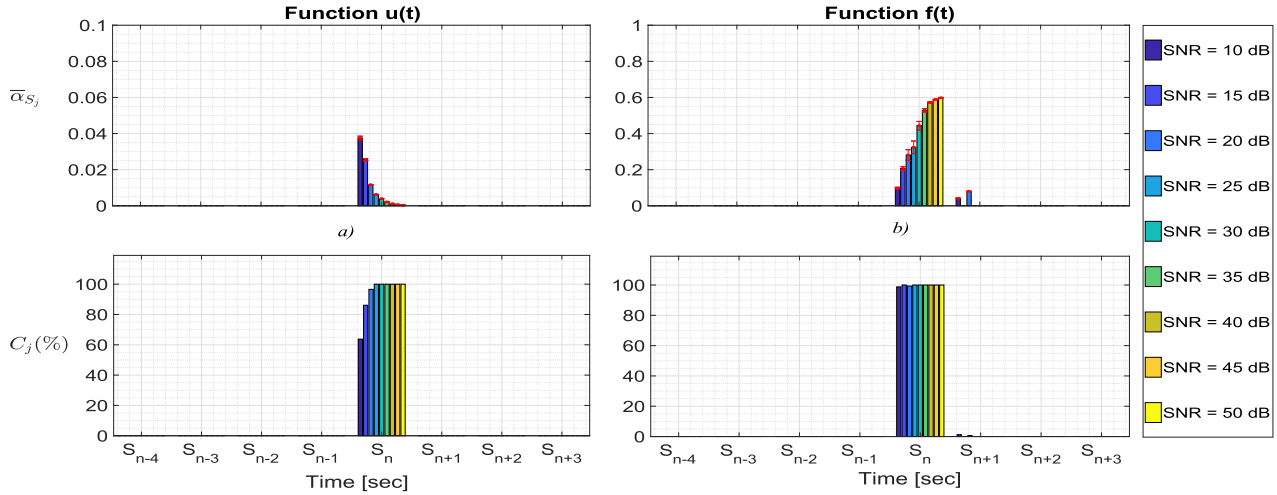


Fig. 4. Mean and standard deviation of Hölder exponent $\bar{\alpha}_{S_j}$ for (a) the step function and (b) monomial function. Bottom panels show the concentration of singularities $C_j(\%)$, respectively.

statistical significance. In addition, the test was used to reject the global null hypothesis (that the mean of the distributions is the same across all the groups being compared), a multiple comparison procedure was also employed to determine which means differ significantly in a pairwise manner. The same procedure was performed separating the sleep in light and deep stages. Finally, the statistical analysis was performed to compare the onset/offset of A-phase against the first window of basal EEG activity.

## III. Results

The results of the analysis of singularities in the EEG signal around A-phase onset/offset are presented. The information is shown for each A-phase sub-type. The singularity strength was measured by the Hölder exponent computed from the Maxima Modules from the scales of the wavelet transformation. To carry out the singularity analysis, we choose as a wavelet function the second derivative of the Gaussian having two vanishing moments, because it presents a good tradeoff between localization and computational cost, and it has been extensively considered to detect singularities [19].

### A. Singularity Detection in Simulated Data

Fig. 4 shows the results of the Hölder exponent, $\alpha$, for $u(t)$ and $f(t)$ functions at different noise levels (bars colors). The analysis was carried out by considering the singularities second-by-second, thus, the signal duration was divided into windows of one second. The number of singularities, as well as the mean and standard deviation of $\alpha$ for the detected singularities at each second, from all the noise realizations, were computed at each window. The location of singularity was defined at the sample 2304 (sampling frequency of 512 Hz), this means the singularity has to be in the second 5, here called $S_n$.

Fig. 4a shows the singularity analysis of the $u(t)$ function. Here again, the localization of the singularity presents a good performance, and for most of the SNR cases, the $\alpha$ strength is close to 0. Thus, the method seems to correctly estimate this singularity type.

In Fig. 4b shows the results of the function (5). We can observe that the location of the singularities was correctly identified for all SNR cases (bottom panel). The $\alpha$ values are close to 0.6 (Figure 4, upper panel) which were correctly measured for SNR higher than 30 dB (yellow bars). Thus, for high noise values, the $\alpha$ value is affected, however, the noise effect does not compromise their identification. This means that the WTMM method is fairly robust to the spurious singularities introduced by noise, as illustrated in the bottom panels.

### B. EEG Singularity Analysis

During the onset and offset of A-phases, at each second $S_j$, we can found various singularities with different Hölder exponent value. Considering $K_{S_j}$ as the number of singularities at each $S_j$ second, the following indexes, for $j = n-2, n-1, n, \ldots, n+4$, were computed:

**Mean of $\alpha$ value:**

$$\bar{\alpha}_{S_j} = \frac{1}{K_{S_j}} \sum_{k=1}^{K_{S_j}} \alpha_{S_j}[k], \tag{6}$$

where $\alpha_{S_j}$ is a Hölder exponent value in the second $S_j$.

**Percentage of change:**

$$\Delta_j(\%) = \bar{\alpha}_{S_j} - \bar{\alpha}_{S_{n-2}}, \tag{7}$$

**Concentration:**

$$C_j(\%) = \frac{K_{S_j}}{K_{S_{n-2}} + K_{S_{n-1}} + \cdots + K_{S_{n+4}}}. \tag{8}$$

Figure 5 shows the dynamics of these features across the onset and offset of A-phases. We employed this strategy since the number of singularities is different at each second. From top to bottom, we present $\bar{\alpha}_{S_j}$, $\Delta_j(\%)$, and $C_j(\%)$, where the blue line represents A1-phase, the orange line corresponds to A2-phase, and the yellow line is the A3-phase, respectively.

The same procedure was applied for the onset and offset. In the case of onset, we observe a statistical increment in

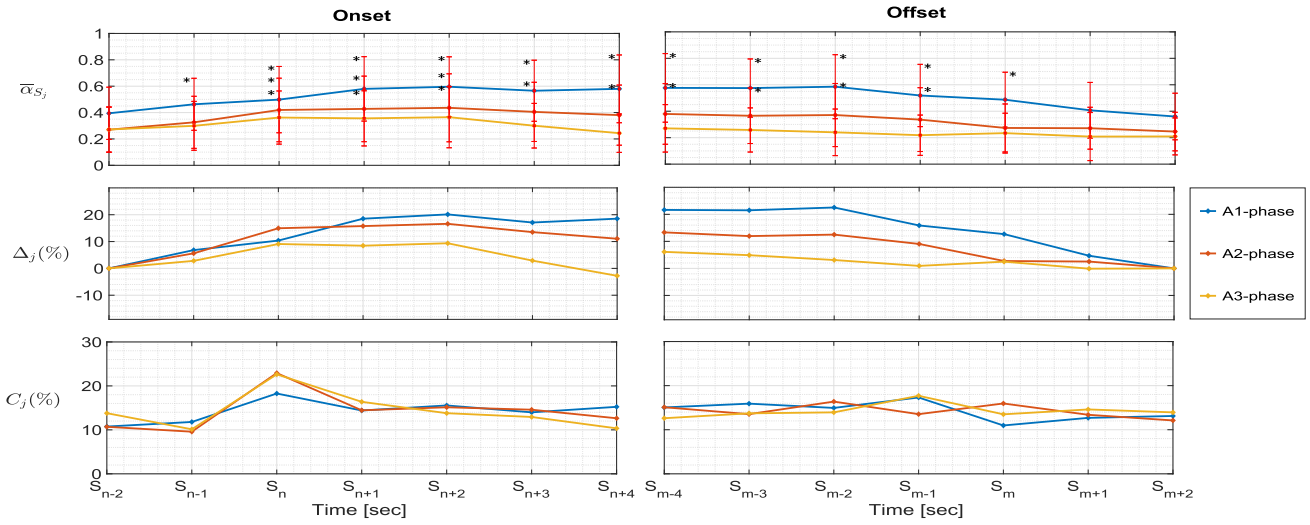


Fig. 5. Singularity indexes of the A-phase sub-type for one healthy subject. For each A-phase sub-type the upper panels show the (mean of the $\alpha$ value) $\bar{\alpha}_{S_j}$ value, the middle panels shows the (percentage of change) $\Delta_j(\%)$ of the Hölder value with respect to the background ($S_{n-2}$ for onset and $S_{m+2}$ for offset). The bottom panels present the (concentration of singularities) $C_j(\%)$ values at each window. The symbol * stands for statistical differences with respect to the background ($S_{n-2}$ for onset and $S_{m+2}$ for offset).

the $\alpha$ when the A-phase starts ($*$ stands for statistical significance with respect to the window $S_{n-2}$), this increment is independent of the A-phase sub-type. However, the $\alpha$ is higher in the A1-phase, which suggests that the singularities are not so strong as the singularities found during A2- and A3-phase. Furthermore, this change in the Hölder value could be better observed in the $\Delta_j(\%)$ value (middle panel), where increments higher than 10% take place from $S_n$. These changes are clearer on the A1-phase and the A2-phase, since most of these phases seem to have similar behavior in the initial part. On the contrary, A3-phases have different waveforms at the onset. Finally, the bottom panel shows that the onset of A-phases has a larger concentration of singularities with respect to any other part, especially the background. By analyzing the offset case, higher $\alpha$ with statistical significance is observed, but just for the A1- and A2-phases ($*$ stands for $p-$value $< 0.05$ with respect to the window $S_{m+2}$). One possible reason for which A3-phases do not show significant changes is that they are usually longer ($>10s$), so the transition from A3-phase to basal activity may occur more smoothly than in the case of A1- or A2-phases. Thus, it seems that the Hölder exponents between EEG background and A3-phases offset are similar. On the other hand, the maximum $\Delta_j(\%)$ value takes place two seconds before the end of the A-phase ($S_{m-2}$), with changes between 20% and 10% for the A1- and A2-phase. Finally, we cannot observe changes in the $\Delta_j(\%)$ value across the offset segments for A3-phase, which suggests that the number of singularities is the same between EEG background and A3-phase offset. Statistical differences were not found when comparing different groups (healthy vs pathological) in a specific second ($S_k$). The behavior of the A-phases, in terms of singularities during onset and offset, are consistent in both groups. Consequently, all A-phase sub-types belonging to healthy and pathological conditions were grouped. Table II shows the behavior of the singularities during the A-phases for all subjects in NREM (HLT_PLM), light sleep (HLT_PLM_LS) and deep sleep (HLT_PLM_DS). The left and right halves of the table show the results, respectively, for the A-phase onset and offset segments. For each group, we present the $\bar{\alpha}_{S_j}$, $\Delta_j(\%)$ and $C_j(\%)$ values. Significantly different values at $S_j$ each index ($p-$value $< 0.05$) with respect to $S_{n-2}$ (for the onset case) and $S_{m+2}$ (for offset case) are shown in bold font. In the upper part of Table II, the HLT_PLM group showed a significant increment in the $\bar{\alpha}_{S_j}$ value at the starting of A1-phase, $S_n$. The $\Delta_j(\%)$ value ranges from 5% to 20% and it is more noticeable in $S_{n+1}$ and $S_{n+2}$. On the other hand, Table II also shows the concentration of the singularity occurrence at each second. We can observe an increment in the occurrence of singularities, specifically in $S_n$. A similar result can be observed during the offset case, but in the opposite direction. Higher values of $\bar{\alpha}_{S_j}$ and a high $C_j(\%)$ are found during the A1-phase. It must be noted that deep sleep is characterized by slow waves similar to the A1-phase waves, in the sense that they present similar frequency content. Nevertheless, there seems to exist differences in the $\Delta_j(\%)$ values and their corresponding $\bar{\alpha}_{S_j}$ values between EEG background and onset/offset of A1-phases for all groups.

The middle part of Table II shows the behavior of the Hölder exponent $\bar{\alpha}_{S_j}$ and the $\Delta_j(\%)$ values during A2-phase. We can observe that A2-phase presents a similar behavior to A1-phase. This means, that higher concentration and $\bar{\alpha}_{S_j}$ values, for both onset and offset cases, occur inside the A2-phase. A different behavior of the singularities is found during the onset and offset of the A3-phase (bottom of Table II). For the onset case, the increment in the $\alpha$ value is not common in all subjects and statistical differences are only found in some cases. In addition, we can observe a large variation in the $\Delta_j(\%)$ value, in fact, from $S_{n+3}$ a decrement in $\alpha$ is observed. However, it is important to note that $S_n$ shows a clear increment in the $\Delta_j(\%)$ values. When analyzing the offset case, no differences are observed between basal EEG and A-phase.

TABLE II

$\bar{\alpha}_{S_j}$, $\Delta_j(\%)$ AND $C_j(\%)$ VALUES FOR ONSET AND OFFSET OF ALL A-PHASE SUB-TYPES. THE BOLD FONT REPRESENTS SIGNIFICANTLY DIFFERENT SEGMENTS, ($p$-VALUE < 0.05) WITH RESPECT TO $S_{n-2}$ (ONSET) OR $S_{m+2}$(OFFSET)

| | | $S_{n-2}$ | $S_{n-1}$ | $S_n$ | $S_{n+1}$ | $S_{n+2}$ | $S_{n+3}$ | $S_{n+4}$ | $S_{m-4}$ | $S_{m-3}$ | $S_{m-2}$ | $S_{m-1}$ | $S_m$ | $S_{m+1}$ | $S_{m+2}$ |
|---|---|---|---|---|---|---|---|---|---|---|---|---|---|---|---|
| ONSET A1 IN NREM | | | | | | | | | OFFSET A1 IN NREM | | | | | | |
| HLT_PLM | $\bar{\alpha}_{S_j}$ | 0.45±0.07 | 0.46±0.07 | **0.52±0.04** | **0.57±0.05** | **0.57±0.06** | **0.55±0.06** | **0.56±0.06** | **0.56±0.06** | **0.55±0.06** | **0.56±0.05** | **0.54±0.05** | 0.49±0.05 | 0.47±0.06 | 0.44±0.05 |
| | $\Delta_j(\%)$ | 0±0 | 1.1±0.1 | **7.6±0.1** | **12.1±0.2** | **12.2±0.2** | **10.5±0.1** | **11.1±0.3** | **11.5±0.2** | **10.8±0.2** | **11.6±0.3** | **9.2±0.2** | **5.2±0.1** | 2.4±0.1 | 0±0 |
| | $C_j(\%)$ | 13±0.01 | 13±0.01 | **16±0.02** | **15±0.02** | **14±0.01** | **15±0.01** | **14±0.01** | **15±0.01** | **15±0.01** | **15±0** | **16±0.02** | 14±0.02 | 13±0.02 | 13±0.01 |
| HLT_PLM_LS | $\bar{\alpha}_{S_j}$ | 0.3±0.07 | 0.34±0.08 | **0.43±0.09** | **0.46±0.06** | **0.43±0.09** | **0.44±0.08** | **0.44±0.08** | **0.46±0.07** | **0.43±0.1** | **0.45±0.11** | **0.42±0.08** | **0.38±0.07** | 0.36±0.08 | 0.33±0.08 |
| | $\Delta_j(\%)$ | 0±0 | 4.6±0.5 | **13.3±0.9** | **16±0.6** | **13.3±1.2** | **13.9±1** | **14.4±0.9** | **13.2±0.8** | **10.3±0.7** | **12±0.6** | **9±0.7** | **5.1±0.4** | 3.4±0.3 | 0±0 |
| | $C_j(\%)$ | 13±0.1 | 13±0.04 | **16±0.06** | **16±0.05** | 13±0.1 | 14±0.06 | 15±0.09 | **15±0.05** | 13±0.09 | **14±0.06** | **17±0.1** | 14±0.06 | 13±0.05 | 14±0.06 |
| HLT_PLM_DS | $\bar{\alpha}_{S_j}$ | 0.49±0.06 | 0.49±0.06 | **0.55±0.04** | **0.6±0.05** | **0.6±0.06** | **0.59±0.05** | **0.59±0.06** | **0.59±0.06** | **0.59±0.05** | **0.59±0.06** | **0.57±0.06** | **0.53±0.05** | 0.5±0.06 | 0.48±0.06 |
| | $\Delta_j(\%)$ | 0±0 | 0.3±0.1 | **6.3±0.2** | **11.7±0.3** | **11.5±0.2** | **9.9±0.1** | **10.4±0.3** | **11.5±0.8** | **10.6±0.7** | **11.4±0.6** | **9.5±0.7** | **5±0.4** | 2±0.3 | 0±0 |
| | $C_j(\%)$ | 13±0.01 | 13±0.01 | **16±0.02** | **15±0.02** | **15±0.02** | **15±0.02** | 14±0.01 | **15±0.01** | **15±0.01** | **15±0.01** | **15±0.02** | 13±0.01 | 14±0.02 | 13±0.01 |
| ONSET A2 IN NREM | | | | | | | | | OFFSET A2 IN NREM | | | | | | |
| HLT_PLM | $\bar{\alpha}_{S_j}$ | 0.33±0.07 | 0.35±0.07 | **0.42±0.06** | **0.44±0.06** | **0.43±0.07** | **0.41±0.07** | **0.4±0.05** | **0.39±0.06** | **0.39±0.05** | **0.39±0.07** | **0.37±0.07** | 0.35±0.07 | 0.33±0.06 | 0.32±0.04 |
| | $\Delta_j(\%)$ | 0±0 | 2.2±0.1 | **9.2±0.1** | **10.4±0.3** | **9.9±0.2** | **7.8±0.3** | **6.4±0.2** | **7.4±0.3** | **6.9±0.2** | **6.9±0.3** | **5.6±0.3** | 3.8±0.2 | 1.6±0.1 | 0±0 |
| | $C_j(\%)$ | 12±0.01 | 12±0.02 | **18±0.04** | **16±0.01** | **14±0.01** | **14±0.01** | **14±0.02** | **14±0.02** | **15±0.02** | **15±0.01** | **15±0.02** | **14±0.02** | 14±0.01 | 13±0.01 |
| HLT_PLM_LS | $\bar{\alpha}_{S_j}$ | 0.29±0.04 | 0.33±0.08 | **0.4±0.06** | **0.4±0.05** | **0.4±0.07** | **0.37±0.07** | **0.36±0.06** | **0.35±0.05** | **0.36±0.06** | **0.35±0.06** | **0.33±0.06** | 0.31±0.05 | 0.3±0 | 0.28±0.04 |
| | $\Delta_j(\%)$ | 0±0 | 4.6±0.3 | **11±0.2** | **11.6±0.2** | **11.5±0.3** | **8.7±0.4** | **7.7±0.2** | **7±0.5** | **7.1±0.9** | **6.6±0.7** | **4.9±0.8** | 2.5±0.5 | 1.6±0.4 | 0±0 |
| | $C_j(\%)$ | 12±0.01 | 12±0.04 | **19±0.06** | **16±0.02** | **14±0.03** | **14±0.01** | **14±0.05** | **14±0.07** | **14±0.04** | **14±0.02** | **16±0.03** | 14±0.02 | 15±0.02 | 13±0.02 |
| HLT_PLM_DS | $\bar{\alpha}_{S_j}$ | 0.41±0.08 | 0.41±0.08 | **0.48±0.07** | **0.5±0.09** | **0.51±0.09** | **0.47±0.07** | **0.45±0.06** | **0.45±0.06** | **0.43±0.07** | **0.45±0.07** | **0.44±0.08** | 0.43±0.11 | 0.4±0.08 | 0.38±0.06 |
| | $\Delta_j(\%)$ | 0±0 | 0.1±0.3 | **7.5±0.1** | **9.1±0.6** | **9.9±0.9** | **5.8±0.6** | 4.1±0.4 | **7.5±0.5** | **5.7±0.9** | **7.8±0.7** | **6.1±0.8** | **5±0.5** | 2.1±0.4 | 0±0 |
| | $C_j(\%)$ | 13±0.05 | 12±0.04 | **18±0.05** | **15±0.06** | **15±0.08** | 14±0.03 | 14±0.12 | 14±0.05 | **14±0.05** | **15±0.03** | **16±0.11** | **15±0.08** | 14±0.05 | 13±0.05 |
| ONSET A3 IN NREM | | | | | | | | | OFFSET A3 IN NREM | | | | | | |
| HLT_PLM | $\bar{\alpha}_{S_j}$ | 0.33±0.06 | 0.35±0.06 | **0.42±0.05** | **0.44±0.05** | **0.43±0.05** | 0.41±0.06 | 0.4±0.05 | 0.25±0.05 | 0.25±0.04 | 0.25±0.06 | 0.25±0.03 | 0.26±0.04 | 0.25±0.04 | 0.25±0.05 |
| | $\Delta_j(\%)$ | 0±0 | 2.1±0.1 | **6.8±0.2** | **7.1±0.2** | **4.5±0.1** | 0.5±0.3 | -2.3±0.3 | 0.4±0.2 | -0.1±0.2 | 0.2±0.2 | -0.1±0.1 | 0.6±0.1 | -0.3±0.1 | 0±0 |
| | $C_j(\%)$ | 14±0.01 | 13±0.03 | **19±0.04** | **16±0.01** | 14±0.01 | 13±0.02 | 12±0.02 | 13±0.03 | 14±0.01 | 14±0.02 | 15±0.01 | 15±0.02 | 15±0.02 | 14±0.02 |
| HLT_PLM_LS | $\bar{\alpha}_{S_j}$ | 0.28±0.06 | 0.3±0.06 | **0.34±0.05** | **0.35±0.05** | **0.32±0.05** | 0.29±0.06 | 0.26±0.05 | 0.24±0.04 | 0.24±0.04 | 0.24±0.05 | 0.24±0.03 | 0.24±0.04 | 0.23±0.04 | 0.24±0.05 |
| | $\Delta_j(\%)$ | 0±0 | 2.2±0.2 | **6.5±0.2** | **6.9±0.3** | **4.2±0.2** | 0.9±0.3 | -1.7±0.3 | -0.1±0.2 | -0.3±0.1 | -0.6±0.3 | 0±0.1 | 0.2±0.1 | -0.6±0 | 0±0 |
| | $C_j(\%)$ | 14±0.01 | 13±0.03 | **19±0.05** | **16±0.02** | 14±0.01 | 13±0.03 | 12±0.03 | **12±0.04** | 14±0.01 | 13±0.03 | 15±0.02 | 15±0.02 | 16±0.03 | 15±0.03 |
| HLT_PLM_DS | $\bar{\alpha}_{S_j}$ | 0.43±0.14 | 0.44±0.11 | **0.47±0.09** | **0.5±0.1** | **0.47±0.1** | 0.41±0.13 | 0.39±0.19 | **0.32±0.1** | 0.31±0.1 | **0.34±0.09** | 0.28±0.09 | 0.32±0.09 | 0.29±0.08 | 0.28±0.09 |
| | $\Delta_j(\%)$ | 0±0 | 1.6±1.6 | **4.6±1.8** | **7.8±1** | 4.5±1.6 | -2.5±0.4 | -2.8±3.2 | 4.7±0.2 | 3.4±0.1 | **6.2±0.3** | 0.2±0.1 | 4.6±0.1 | 1.1±0 | 0±0 |
| | $C_j(\%)$ | 14±0.2 | 12±0.18 | **18±0.14** | **16±0.29** | 14±0.15 | 14±0.06 | 13±0.16 | 14±0.29 | 13±0.22 | 13±0.23 | **16±0.43** | 14±0.23 | **17±0.38** | 12±0.33 |

### C. Discriminative Properties of Singularities

In Biomedical Engineering, it is of great relevance to understand whether the information extracted from physiological signals helps to automatically detect a medical condition. Given the importance of exploring new features that could improve the classification procedure, it is interesting to study whether the EEG singularity, around the onset of A-phase, is a discriminative feature. For this purpose, $\bar{\alpha}_{S_j}$ and $C_j(\%)$ values in the second $S_{-2}$ (class BKGRND) and the second $S_1$ (class ONSET), of the A-phase onset were used as inputs to a multilayer shallow neural network (NN) with backpropagation training. Table III shows the confusion matrix and the Cohen's kappa index of the test results of the NNs with an architecture of two inputs, four hidden (transfer function: sigmoid) and one output (transfer function: sigmoid), and the mean square error as a performance function. We evaluated the following cases: a) all the A-phases, b) A-phases in deep or light sleep, and c) A-phases by subtype. Other architectures were also evaluated varying the hidden layer from 2 to 10 neurons. In each case, 10 different NNs were trained and tested by taking 90% of the data for training and 10% for testing. Samples from each set were randomly selected each time that a new NN was trained. To ensure that the classification results are produced by the presence of the A-phases, the values of the singularities of all A-phases were randomly re-ordered, and the training and testing (SURROGATE) procedures were performed again. From Table III, it is observed that results evaluated via the kappa coefficient for the surrogate data is very small, while for the real data it is at least one order of magnitude higher. In addition, the singularities present a moderate level of discriminative power, therefore it could be used as a complement to other features already used in the literature. As expected classification with surrogate sets is not possible and this helps to show that the singularity around the onset of A-phase is related to the occurrence of the event. Furthermore, other strategies based on singularities could be evaluated to improve the classification task, for instance, the highest singularity value, or take into account singularities considering more seconds, among others.

### D. Analysis of Individual Variability

Table IV shows the statistical analysis of the singularities behavior during A-phases for each subject in NREM (HLT_PLM), light sleep (HLT_PLM_LS) and deep sleep (HLT_PLM_DS). The left and right halves of the table show the results, respectively, for the A-phase onset and offset segments. Please note that this analysis is similar to the one performed in the EEG singularity analysis Section. This analysis was carried out per subject with the aim to quantify the individual variability. Each cell contains the percentage of subjects with significance difference in a second $S_j$ and $S_k$ with respect to $S_{n-2}$ and $S_{m-4}$, respectively, where $j = n-1, n, \ldots, n+4$, and $k = m-3, m-2, \ldots, m+2$, please see Fig. 1. In bold font are shown the seconds where more than 75% of the subjects have statistical difference. At first on the onset segment, it is observed that most of the subjects present statistical difference for the A1-phase from $S_{n+1}$ second for all the cases. This suggests that A1-phase modifies the EEG

TABLE III
CONFUSION MATRIX FOR THE TEST RESULTS OF THE NNS PERFORMANCE FOR THE A-PHASE ONSET CLASSIFICATION BASED ON TRUE AND SURROGATE SINGULARITIES

| TRUE A-phase | | | | | | |
|---|---|---|---|---|---|---|
| | **ALL** | | **DEEP SLEEP** | | **LIGHT SLEEP** | |
| | **ONSET** | **BKGRND** | **ONSET** | **BKGRND** | **ONSET** | **BKGRND** |
| **ONSET** | 2854 | 2246 | 1158 | 852 | 1916 | 1174 |
| **BKGRND** | 2018 | 3082 | 833 | 1177 | 1557 | 1533 |
| **kappa coefficient** | 0.1666 | | 0.1214 | | 0.1432 | |
| | **A1-phase** | | **A2-phase** | | **A3-phase** | |
| **ONSET** | 1037 | 819 | 707 | 547 | 1054 | 934 |
| **BKGRND** | 802 | 1052 | 510 | 746 | 917 | 1065 |
| **kappa coefficient** | 0.1416 | | 0.1690 | | 0.1366 | |
| SURROGATE | | | | | | |
| | **ALL** | | **DEEP SLEEP** | | **LIGHT SLEEP** | |
| | **ONSET** | **BKGRND** | **ONSET** | **BKGRND** | **ONSET** | **BKGRND** |
| **ONSET** | 2510 | 2590 | 953 | 1057 | 1608 | 1482 |
| **BKGRND** | 2493 | 2607 | 988 | 1022 | 1600 | 1490 |
| **kappa coefficient** | 0.0148 | | 0.0244 | | 0.0068 | |
| | **A1-phase** | | **A2-phase** | | **A3-phase** | |
| **ONSET** | 870 | 984 | 558 | 697 | 876 | 1109 |
| **BKGRND** | 822 | 1034 | 580 | 675 | 881 | 1104 |
| **kappa coefficient** | 0.0028 | | -0.0138 | | -0.023 | |

TABLE IV
PERCENTAGE OF SUBJECTS WITH SIGNIFICANCE DIFFERENCE AT EACH SECOND DURING THE ONSET AND OFFSET OF A-PHASES

| | Seconds → | $S_{n-2}$ | $S_{n-1}$ | $S_n$ | $S_{n+1}$ | $S_{n+2}$ | $S_{n+3}$ | $S_{n+4}$ | $S_{m-4}$ | $S_{m-3}$ | $S_{m-2}$ | $S_{m-1}$ | $S_m$ | $S_{m+1}$ | $S_{m+2}$ |
|---|---|---|---|---|---|---|---|---|---|---|---|---|---|---|---|
| Case | Type | Onset | | | | | | | Offset | | | | | | |
| HLT_PLM | A1 | 0 | 16 | 63 | **89** | **89** | **89** | **84** | **89** | **95** | **84** | **84** | 47 | 05 | 0 |
| | A2 | 0 | 11 | **84** | **89** | **89** | 68 | 63 | 63 | 58 | 47 | 58 | 32 | 16 | 0 |
| | A3 | 0 | 05 | 63 | 58 | 37 | 11 | 11 | 11 | 16 | 05 | 0 | 0 | 05 | 0 |
| HLT_PLM_LS | A1 | 0 | 47 | **79** | **84** | **89** | **89** | **89** | **89** | **79** | **79** | 68 | 58 | 42 | 0 |
| | A2 | 0 | 21 | **95** | **1** | **1** | 74 | 68 | 42 | 68 | 53 | 53 | 21 | 05 | 0 |
| | A3 | 0 | 21 | 63 | 63 | 37 | 16 | 21 | 21 | 11 | 16 | 05 | 16 | 0 | 0 |
| HLT_PLM_DS | A1 | 0 | 11 | 63 | **89** | **84** | **95** | **84** | **89** | **79** | **79** | **84** | 37 | 16 | 0 |
| | A2 | 0 | 26 | 68 | 74 | 53 | 42 | 47 | 58 | 53 | 79 | 68 | 37 | 21 | 0 |
| | A3 | 0 | 53 | 68 | 68 | 68 | 47 | 47 | 47 | 58 | 74 | 47 | 47 | 42 | 0 |

composition after one second of the A-phase onset. For the A2-phase, most of the subjects present statistical difference in the first three seconds of the A-phase onset, except for the deep sleep case. Finally, A3-phase does not generate any statistical difference in most of the subjects. On the other hand, in the previous seconds of the offset segment, most of the subjects during the A1-phase showed statistical difference. These results are in agreement with those of Table II.

## IV. DISCUSSION

The analysis of singularities in the EEG signal around the A-phase onset and offset was presented. The singularities were evaluated by the Maximum Module of the wavelet decomposition. Our main observations are: a) EEG presents a high content of singularities during the basal fluctuations of the sleep stages, and b) the singularities of EEG around A-phases seem independent of the subject condition.

The results provide evidence that the EEG signal presents singularities during NREM sleep. These occur during the basal oscillations of the different sleep stages and also during the A-phases, but with different Hölder value. It is interesting since these results supports the idea that the A-phases have different dynamics with respect to the background activity, even when their frequency content is similar. Specifically, this is better appreciated during deep sleep, where the EEG oscillation is predominantly in the low part of the spectrum (delta band), which is similar to the A1-phase spectral content. Furthermore, an interesting outcome of this analysis arises from the comparison of A-phase singularities between healthy and pathological sleep. Although there is a different number of A-phases between the healthy and pathological groups

of subjects, the Hölder exponent and the behavior of the singularities across the analyzed segments were very similar and no significant differences were observed between these two groups. This suggests a consistent behavior of A-phases, in both healthy and pathological sleep conditions. When considering the singularities in light sleep and deep sleep separately, it is worth noting a significant change (about 10%) of the Hölder exponent during the A-phases. This suggests that the behavior of the singularities during the A-phases are depends on the sleep stage in which they occur.

From the results, it seems the A-phase onset generally presents an increment of singularities for all A-phase subtype. A similar behavior is observed during the offset with the exception of A3-phase. The results complement previous studies, such as, the work carried out by De Carli *et al.* [30]. They found significant changes in the spectral content of the background activity and the A phases, even in cases where the A-phases and background activity present a similar behavior. Similarly, in [12], the authors present evidence of a clear change in energy, power, entropy, and standard deviation between background activity and the onset of A1- and A2-phases. Concerning the A3-phases, our results are in agreement with previous work [12], since the analysis of the Hölder exponent at the offset of these phases did not show a consistent significant change, which could be related to the long duration and variability of the A3-phases.

On the other hand, the identification of A-phases can be a complicated task since there exist EEG sections with very similar characteristics to the changes generated by A-phases which produce false positives. However, the method used in this study from a practical point of view could be part of more complex algorithms to help the detection of onset of A-phases and try to decrease the number of false positives. Our results did not give an insight of a singularity correlated to the precise time of clinician offset annotations. It suggests that A-phase could involve a series of processes inside the brain structures and the integration of a large number of neurons move smoothly toward the new state, this is why we believe that the change observed as a sudden transition, does not convey a singularity. This follows the idea of the authors in [31], where they mention that the A-phases are considered as an oscillation and not a pulse.

The sampling frequency is an issue that needs to be carefully analyzed. This is because clinicians generally consider the frequency content of the EEG to annotate the sleep stages and short cortical events. The sleep clinician usually considers the frequency bands in the range between 0.05 Hz to 30 Hz; only in cognitive tasks frequencies go up to 80 Hz. However, singularity analysis benefits from a high frequency sampling rate to capture the punctual changes that generate singularities. If a low sampling rate is used, the singularities might not be adequately represented.

We analyzed records with different sampling rates (100 Hz, 128 Hz, 200 Hz, and 512 Hz), and we observed a clear difference in the ability to detect singularities between low resolution recordings (100 Hz, 128 Hz) and high resolution recordings (200 Hz and 512 Hz). Specifically, the recordings of low resolution show a reduced number of singularities with respect to the high resolution recordings. It is important to comment that the singularities are lost in the low resolution recording and could not be recovered for any mathematical method since the information is not captured. On the other hand, the high resolution can considerably increase the occurrence of singularities caused by noise, but the method used in this study is quite robust and manages to eliminate most of the unwanted information, which could be observed in the experiment with synthetic signals.

The EEG signal is often contaminated by noise, or by the interference of other physiological signals such as ECG, resulting in spurious singularities. It could be argued that this would produce a similar number of singularities in the onset/offset and the background. However, this study showed a statistical difference of singularities between A-phases and background; which suggests this particular behavior in the EEG dynamics is related to the A-phase. It is important to observe that a standard filtering process could be applied to reduce the noise levels, but the singularities could be smoothed out or completely destroyed by most filtering strategies.

The numerical results obtained with the wavelet singularity analysis suggest that the Hölder exponent can be considered as a marker of the local changes in EEG dynamics during A-phases. This allows an alternative characterization of the A-phases that could help to develop automatic methods for their detection. Since the length of data is large (around 8 hours), we decided to use the WTMM method with the second derivative Gaussian function as a wavelet to obtain a better localization accuracy with an acceptable computational cost. Finally, two possible veins for further study are derived from the current work. The first one is to evaluate which wavelet function with different number of vanishing moments presents a better performance to characterize the different sleep stages. The second one is the multifractal analysis that may be helpful to characterize the relationship among neighboring singularities.

## V. Conclusion

The characterization of EEG signals based on singularities and their strength during A-phases based on Hölder exponent was carried out. The EEG signal presented singularities inside and outside the A-phases, which suggests abrupt changes in the EEG during sleep. Additionally, during the A-phases a higher number of singularities occurs suggesting a different cerebral process, especially in A1- and A2-phases. These findings contribute to understanding the effect of A-phases on EEG signal and open the opportunity to develop a different characterization of the CAP phenomenon. The computation of the Hölder exponent based on wavelet decomposition seems to be a useful tool for this task, where the per-subject analysis shows consistent results for A1-phases. As a final remark, the singularity analysis alone does not seem to provide enough information for accurately detecting A-phases; however, all A-phase features proposed so far suffer from this issue.

## Appendix
## Continuous Wavelet Transform

The basic concepts of the continuous wavelet transform for singularity detection are presented in this appendix.

Let $L^2(\mathbb{R})$ denotes the space of all square-integrable functions on $\mathbb{R}$, and let $\psi(t) \in L^2(\mathbb{R})$ be a fixed function.
We define the continuous wavelet transform (WT) of a signal $f(t) \in L^2(\mathbb{R})$ by

$$W_f(s, t_0) = \frac{1}{\sqrt{s}} \int_{-\infty}^{\infty} f(t) \bar{\psi} \left( \frac{t - t_0}{s} \right) dt, \tag{9}$$

where $\psi$ is the analyzing wavelet, $t_0 \in \mathbb{R}$ is a translation parameter, whereas $s \in \mathbb{R}^+$ $(s \neq 0)$ is a dilation or scale parameter, and the bar symbol denotes complex conjugation. In order to analyze appropriately the singular behavior of a function, signal or distribution, the wavelet functions $\psi(t)$ should have enough vanishing moments [27], [29], [32]. A wavelet function is said to have $n$ vanishing moments if and only if it satisfies

$$\int_{-\infty}^{\infty} t^k \psi(t) dt = 0, \tag{10}$$

for $k = 0, 1, \ldots, n-1$, and

$$\int_{-\infty}^{\infty} t^k \psi(t) dt \neq 0 \quad \text{for } k = n. \tag{11}$$

This means that a wavelet with $n$ vanishing moments is orthogonal to all polynomials of degrees up to $n-1$.

In addition, the concept of cone of influence is crucial in the singularity analysis. Let us assume that $\psi$ is non-zero in the interval $[-C, C]$. The cone of influence of $\psi$ at point $t_0$ is the set of points $(s, t)$ in the scale-space plane, such that $t_0$ is in the support of $\psi\left((t - t_0)/s\right)$. Since the support of $\psi\left((t - t_0)/s\right)$ is the set of points in the interval $[t_0 - Cs, t_0 + Cs]$, the point $(s, t)$ belongs to the cone of influence of $t_0$ if

$$|t - t_0| \leq Cs. \tag{12}$$

## REFERENCES


[1] B. M. Altervogt and H. R. Colten, *Sleep Disorders and Sleep Deprivation: An Unmet Public health problem*. Washington, DC, USA: Academies, 2006.

[2] C. Iber, S. Ancoli-Israel, A. Chesson, S. F. Quan, "The AASM manual for the scoring of sleep and associated events: Rules, terminology and technical specifications," Amer. Acad. Sleep Med., Westchester, IL, USA, 2007.

[3] V. E. Arce-Guevara, M. O. Mendez, J. S. Murguía, A. Alba, H. González-Aguilar, and E. R. Palacios-Hernández, "Scaling analysis of the A-phase dynamics during sleep," *Fractals*, vol. 28, no. 2, 2020, Art. no. 2050050.

[4] A. Rechtschaffen and A. Kales, "A manual of standardized terminology, techniques and scoring system for sleep stages of human subjects," U.S. Nat. Inst. Neurological Diseases Blindness, Neurological Inf. Netw., 1968.

[5] M. G. Terzano *et al.*, "Atlas, rules, and recording techniques for the scoring of cyclic alternating pattern (CAP) in human sleep," *Sleep Med.*, vol. 3, no. 2, pp. 187–199, Mar. 2002.

[6] M. G. Terzano and L. Parrino, "Clinical applications of cyclic alternating pattern," *Physiol. Behav.*, vol. 54, no. 4, pp. 807–813, Oct. 1993.

[7] R. Ferri, O. Bruni, S. Miano, A. Smerieri, K. Spruyt, and M. G. Terzano, "Inter-rater reliability of sleep cyclic alternating pattern (CAP) scoring and validation of a new computer-assisted cap scoring method," *Clin. Neurophysiol.*, vol. 116, no. 3, pp. 696–707, 2005.

[8] S. Mariani *et al.*, "Characterization of A-phases during the cyclic alternating pattern of sleep," *Clin. Neurophysiol.*, vol. 122, no. 10, pp. 2016–2024, 2011.

[9] C. Navona, U. Barcaro, E. Bonanni, F. Di Martino, M. Maestri, and L. Murri, "An automatic method for the recognition and classification of the A-phases of the cyclic alternating pattern," *Clin. Neurophysiol.*, vol. 113, no. 11, pp. 1826–1831, Nov. 2002.

[10] U. Barcaro, E. Bonanni, M. Maestri, L. Murri, L. Parrino, and M. G. Terzano, "A general automatic method for the analysis of NREM sleep microstructure," *Sleep Med.*, vol. 5, no. 6, pp. 567–576, 2004.

[11] S. Mariani *et al.*, "Efficient automatic classifiers for the detection of A phases of the cyclic alternating pattern in sleep," *Med. Biol. Eng. Comput.*, vol. 50, no. 4, pp. 359–372, 2012.

[12] M. O. Mendez *et al.*, "Analysis of A-phases transitions during the cyclic alternating pattern under normal sleep," *Med. Biol. Eng. Comput.*, vol. 54, no. 1, pp. 133–148, 2015.

[13] S. Dhok, V. Pimpalkhute, A. Chandurkar, A. A. Bhurane, M. Sharma, and U. R. Acharya, "Automated phase classification in cyclic alternating patterns in sleep stages using Wigner–Ville distribution based features," *Comput. Biol. Med.*, vol. 119, Apr. 2020, Art. no. 103691.

[14] T. Fantozzi, M. Paola, U. Faraguna, A. Ugon, G. Ciuti, and A. Pinna, "Automatic cyclic alternating pattern (CAP) analysis: Local and multi-trace approaches," *PLoS ONE*, vol. 16, no. 12, 2021, Art. no. e0260984.

[15] E. R. Arce-Santana, A. Alba, M. O. Mendez, and V. Arce-Guevara, "A-phase classification using convolutional neural networks," *Med. Biol. Eng. Comput.*, vol. 58, no. 5, pp. 1003–1014, 2020.

[16] S. Murarka, A. Wadichar, A. Bhurane, M. Sharma, and U. R. Acharya, "Automated classification of cyclic alternating pattern sleep phases in healthy and sleep-disordered subjects using convolutional neural network," *Comput. Biol. Med.*, vol. 146, May 2022, Art. no. 105594.

[17] S. Hartmann and M. Baumert, "Automatic A-phase detection of cyclic alternating patterns in sleep using dynamic temporal information," *IEEE Trans. Neural Syst. Rehabil. Eng.*, vol. 27, no. 9, pp. 1695–1703, Sep. 2019.

[18] F. Mendonça, S. S. Mostafa, F. Morgado-Dias, and A. G. Ravelo-García, "On the use of patterns obtained from LSTM and feature-based methods for time series analysis: Application in automatic classification of the CAP A phase subtypes," *J. Neural Eng.*, vol. 18, no. 3, 2021, Art. no. 036004.

[19] S. Mallat and W. L. Hwang, "Singularity detection and processing with wavelets," *IEEE Trans. Inf. Theory*, vol. 38, no. 2, pp. 617–643, Mar. 1992.

[20] P. Venkatakrishnan and S. Sangeetha, "Singularity detection in human EEG signal using wavelet leaders," *Biomed. Signal Process. Control*, vol. 13, pp. 282–294, 2014.

[21] A. Vena, E. Conte, G. Perchiazzi, A. Federici, R. Giuliani, and J. P. Zbilut, "Detection of physiological singularities in respiratory dynamics analyzed by recurrence quantification analysis of tracheal sounds," *Chaos, Solitons Fractals*, vol. 22, no. 4, pp. 869–881, Nov. 2004.

[22] E. Conte, V. Antonio, F. Antonio, G. Rocco, and P. Z. Joseph, "A brief note on possible detection of physiological singularities in respiratory dynamics by recurrence quantification analysis of lung sounds," *Chaos, Solitons Fractals*, vol. 21, no. 4, pp. 869–877, 2004.

[23] J. P. Zbilut, M. Zak, and C. L. Webber, Jr., "Physiological singularities in respiratory and cardiac dynamics," *Chaos, Solitons Fractals*, vol. 5, no. 8, pp. 1509–1516, Aug. 1995.

[24] P. Zhan *et al.*, "R-wave singularity: A new morphological approach to the analysis of cardiac electrical dyssynchrony," *Frontiers Physiol.*, vol. 11, Dec. 2020, Art. no. 599838.

[25] E. W. Abel, H. Meng, A. Forster, and D. Holder, "Singularity characteristics of needle EMG IP signals," *IEEE Trans. Biomed. Eng.*, vol. 53, no. 2, pp. 219–225, Feb. 2006.

[26] K. Marri and S. Ramakrishnan, "Classification of muscle fatigue in dynamic contraction using surface electromyography signals and multifractal singularity spectral analysis," *J. Dyn. Syst., Meas., Control*, vol. 138, no. 11, 2016, Art. no. 111008.

[27] S. Mallat, *A Wavelet Tour of Signal Processing*. New York, NY, USA: Academic Press, 1999.

[28] J. S. Murguía and J. Urías, "On the wavelet formalism for multifractal analysis," *Chaos, Interdiscipl. J. Nonlinear Sci.*, vol. 11, no. 4, pp. 858–863, 2001.

[29] J. F. Muzy, E. Bacry, and A. Arneodo, "The multifractal formalism revisited with wavelets," *Int. J. Bifurcation Chaos*, vol. 4, no. 2, pp. 245–302, Apr. 1994.

[30] F. De Carli *et al.*, "Quantitative analysis of sleep eeg microstructure in the time-frequency domain," *Brain Res. Bull.*, vol. 63, no. 5, pp. 399–405, 2004.

[31] M. G. Terzano and L. Parrino, "Origin and significance of the cyclic alternating pattern (CAP)," *Sleep Med. Rev.*, vol. 4, no. 1, pp. 101–123, 2000.

[32] I. Daubechies, "Ten lectures on Wavelets," in *Society for Industrial and Applied Mathematics*. Philadelphia, PA, USA: SIAM, 1992.